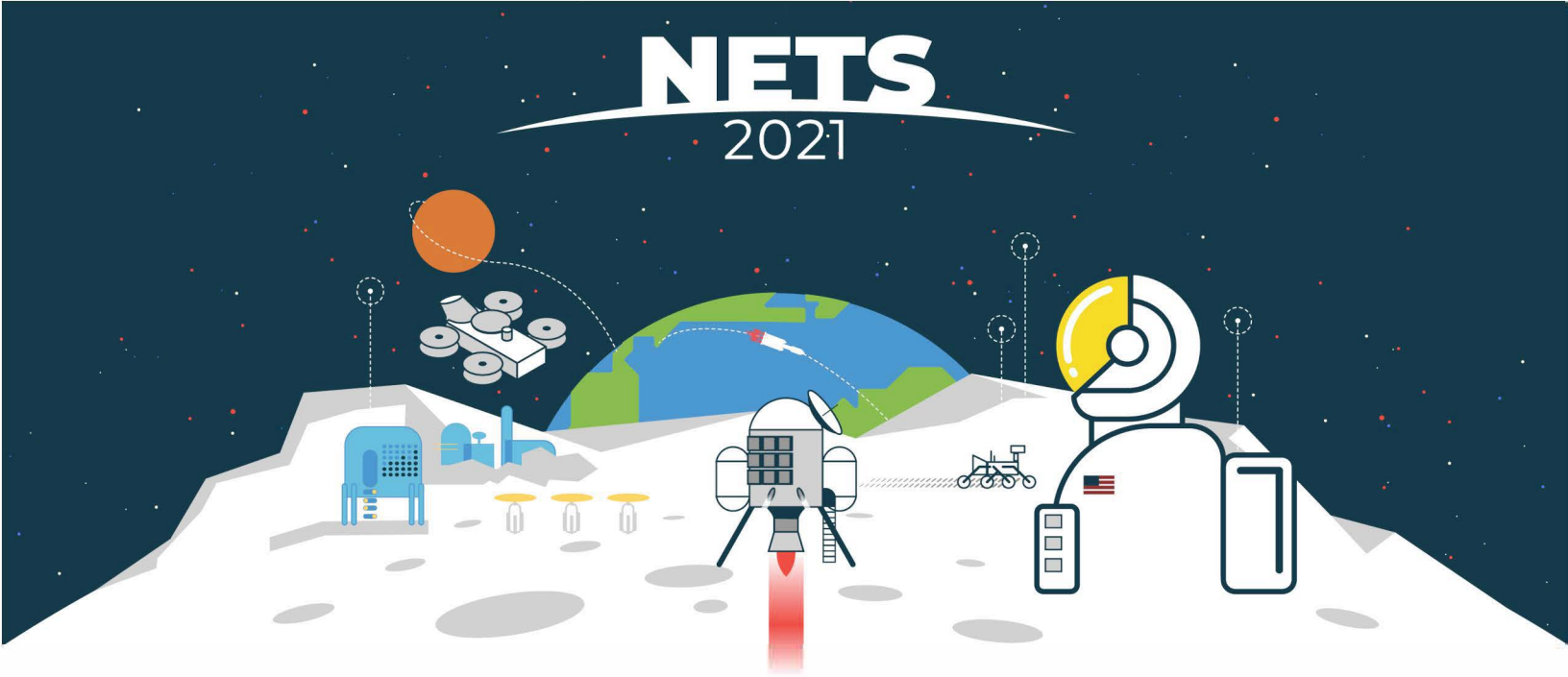

NUCLEAR and
EMERGING
TECHNOLOGIES for
SPACE

CONFERENCE PROCEEDINGS

Hosted by Oak Ridge National Laboratory

April 26th-30th, 2021

Track 4: Advanced and Emerging Technologies for Nuclear Space Applications

Technical Track Chair(s): Steve Howe & Gerry Jackson

U.S. DEPARTMENT OF ENERGY

https://nets2021.ornl.gov

OAK RIDGE National Laboratory

Author	Title
Floyd, Dan C.	Planned Steady State Irradiation of Characterized Instruments for Nuclear Thermal Rockets Using In-Pile Experiment Apparatus
Morris, Nicholas A.	A Cool Model to Analyze Heat Deposition on MTV Propellant Tanks
Puri, Rohan	Helicon Injected Inertial Plasma Electrostatic Rocket

Nuclear and Emerging Technologies for Space
Sponsored by Oak Ridge National Laboratory, April 26th-30th, 2021.
Available online at https://nets2021.ornl.gov

PLANNED STEADY STATE IRRADIATION OF CHARACTERIZED INSTRUMENTS FOR NUCLEAR THERMAL ROCKETS USING IN-PILE EXPERIMENT APPARATUS

Dan C. Floyd[1], Tyler R. Steiner[1], Emily Hutchins[1], N. Dianne Bull Ezell[2], and Richard Wood[1]

[1]*University of Tennessee, Knoxville, TN, 37996-1410*
[2]*Oak Ridge National Laboratory, Oak Ridge, TN, 37831*

Primary Author Contact Information: dfloyd7@vols.utk.edu

The development of nuclear rocket technology is critical for the further exploration of extraterrestrial bodies. Nuclear rockets are capable of providing various advantages over current chemical rockets. However, the harsh environment provides a number of challenges regarding instrument performance. Temperature extremes, radiation (reactor and space), and the inability to conduct traditional maintenance activities can lead to a severe degradation in instrument performance. To better understand the effects of radiation on instrumentation, an irradiation campaign has been designed to test a set of instruments provided by a collaborator in the aerospace industry. Details concerning pre-irradiation performance are provided for a future comparison to the irradiated performance. Additionally, the design of the irradiation test is described in detail.

I. INTRODUCTION

Nuclear thermal propulsion produces severe environments and requires accurate measurements over extended periods of time. However, there is limited opportunity for maintenance and calibration drift can prove disastrous for mission success. In addition to this, the instrumentation needs to maintain performance and functionality after long exposures to nuclear radiation. While the total exposure will vary with installation location, historical documents indicate a possible range of 10^{18} nvt to 10^{21} nvt over the mission lifetime [1, 2]. As such, the performance of instrumentation when exposed to extreme temperatures and radiation needs to be evaluated.

Several instruments that have been implemented in aerospace investigations have been acquired to provide an initial investigation. The sensors of interest consist of 4 different pressure transducers, a flowmeter, and 4 platinum resistance temperature detectors (RTDs). As several of the pressure and temperature instruments are of similar model and construction, a representative sensor was chosen for each available model. The results of the non-irradiated evaluation and a post irradiation examination can be compared to determine any effects due to irradiation or temperature exposure.

The performance of the pressure and flow instruments was determined through the implementation of a simple flow path with a 90psig max pressure supply. The pressure ranged from 0-90psig through the manipulation of a manual pressure regulator valve. A single measurement run is considered to encompass measurements as the pressure is increased by steps of 10psi until the maximum and then decreased until it has attained the minimum value. This is then repeated to provide 3 runs in total for each pressure sensor. Additionally, several configurations of the sensors being powered on and off were conducted. For simplicity, the pressure transducers are indicated as S206 and S217. This allows for crosstalk and interferences between the sensors to be determined and removed from the output signal. Data collection should provide the necessary information regarding instrument performance.

II. CHARACTERIZATION

II.A. Pressure Sensor Performance

The output of the pressure transducers is miniscule (30mV) and susceptible to noise. As the maximum pressure provided to the transducers is ~90psig, the maximum value of S217 is close to the maximum output of the sensor. Additionally, the S217 has noticeable noise but it appears to be within a reasonable limit. However, S206 is severely affected by noise. A similar noise signal is present on the implemented reference sensor, but the larger magnitude output provides a more favorable signal to noise ratio.

The calibration curve of the pressure transducers is constructed using a least square regression to determine the calibration coefficients. The calibration curve of each pressure sensor can be seen in Figures 1 and 2. The S206 pressure transducer has significant issues regarding the noise. Part of this can be improved by implementing a low-pass filter around 60Hz. This would remove the 60Hz voltage ripple from the power supply caused by rectifying an alternating current. Additionally, it is possible to remove some amounts of noise by using the cross-power spectral density of some of the collected signals. However, this is not a critical need for this work due the fact that only a simple comparison is required regarding performance.

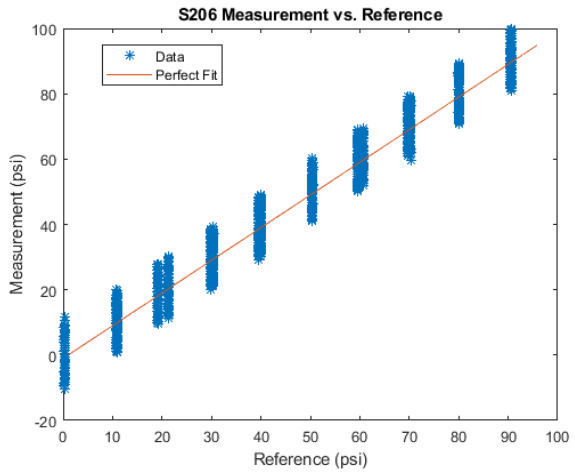

Fig. 1: S206 measurement versus the reference pressure.

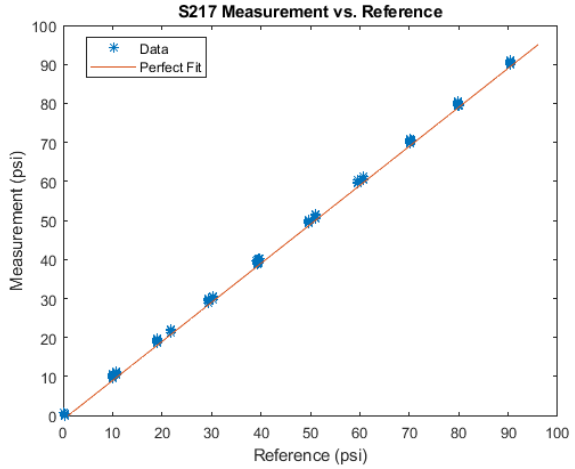

Fig. 2: S217 measurement versus the reference pressure.

II.B. Flowmeter Performance

The provided flowmeter uses a standard 0-5VDC output with a measurement range of 0-50LPM. The necessary data regarding the sensor was determined using a calibrated mass flow controller with a built-in meter to provide a reference. The data collection started with a 30 second hold at a minimum point of 0LPM which was then increased by 20LPM over 60 seconds and held for 30 seconds. This is repeated until the maximum flow of the controller is reached and then a similar process returns the flow to the initial point. A comparison of the flowmeter measurement with respect to the reference flow measurement is available in Figure 3. Quantitatively, the error of the curve can be described by the RMSE which has a value of ±0.652.

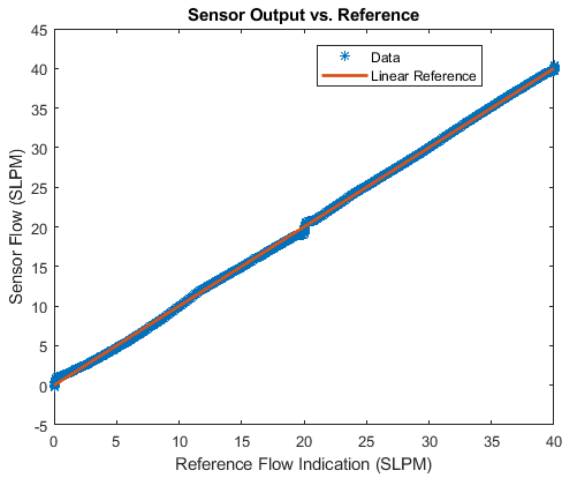

Fig. 3: Instrument measurement versus reference.

II.C. Temperature Sensor Performance

The provided temperature instrument is a platinum resistance temperature detector (RTD) with a nominal resistance of 500Ω and a measurement range of -18°C–93°C. Generally, front-end electronics are required to convert the resistance change into a voltage or current signal. This particular model does not require additional electronics due to specialized circuit embedded in the head of the RTD. This allows for a 10V power supply and a simple DAQ to be implemented in temperature measurements.

The sensitivity of the instrument when it was constructed was 4mV/V, which provides an output range if 0-40mV when supplied with 10VThe current calibration curve for the instrument was developed using a rudimentary calibration set up. The output voltage of the instrument was measured in an ice bath, stable room temperature, and at the boiling point of water. Exact temperatures are determined through the usage of a calibrated Pt-100Ω RTD that conforms to the Class A accuracy stated in IEC 60751. A least square regression using the voltage and reference temperature value provides the needed calibration coefficients.

From Figure 4, the largest percent change in the curve is ~0.073%, indicating minimal change from the original curve. Additionally, Figure # provides a visual method to match the measure voltage with the reference temperature. Quantitatively, this can be defined using the root mean square error (RMSE) of the prediction. The RMSE using the provided calibration coefficients is ±0.117.

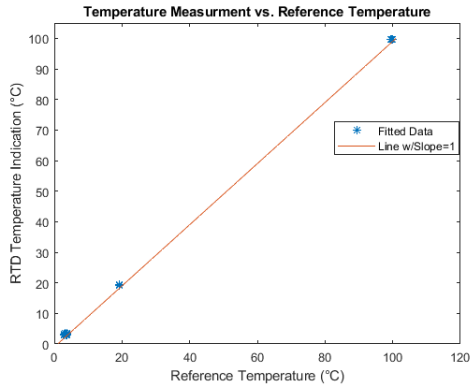

Fig. 4: RTD measurement versus reference temperature.

III. IRRADIATION TEST PLAN

III.A Flow and High temperature test

The irradiation of the instruments will take place within the Ohio State University Research Reactor (OSURR). Due to the number of instruments, the instrumentation is being spread across two irradiation periods. To inform safe handling and shipping of the irradiated experiments, a neutron activation analysis will be performed using the Monte Carlo N-Particle (MCNP) and Oak Ridge Isotope Generation (ORIGEN) codes. The stainless-steel components that make up the power CF flange passthrough, thermocouple CF flange passthroughs, and the flow meters are the greatest activation concern for these experiments.

As the flow meters can interfere with the measurements from the pressure transducers, the initial test focuses solely on flow measurement. The test is to be conducted using helium as the process fluid at ambient temperature and pressure. This allows the benchtop tests to be recreated with minimal changes. This includes a similar process for data collection and setpoint variation as conducted during the pre-irradiation characterization. Figure 5 provides a simple graphic showing the expected volumetric flow rate and reactor power level over the irradiation period.

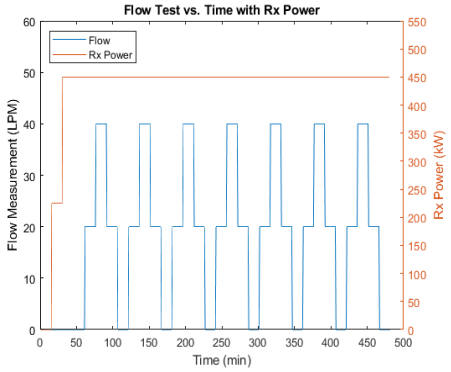

Fig. 5: Planed flow variation over the irradiation test period.

To optimize utilization of the OSURR, the In-Pile Experiment Set Apparatus (INSET) will also be demonstrated during this initial test. INSET is a high temperature, in-pile, steady-state testbed for nuclear thermal propulsion (NTP) experiments [3]. INSET will serve as the furnace for the heated pressure sensor test. For the first instrument test, the flow meters will be distanced from the heater within INSET to eliminate any heating effects on the instruments. INSET will be heated to 2000°C during reactor operation. INSET will maintain this temperature for 30 minutes near the end of the irradiation period, as shown in Figure 6. The high temperature test will demonstrate that INSET can meet the need for high temperature, steady state, in-pile experimental testing that is not currently met for NTP interests.

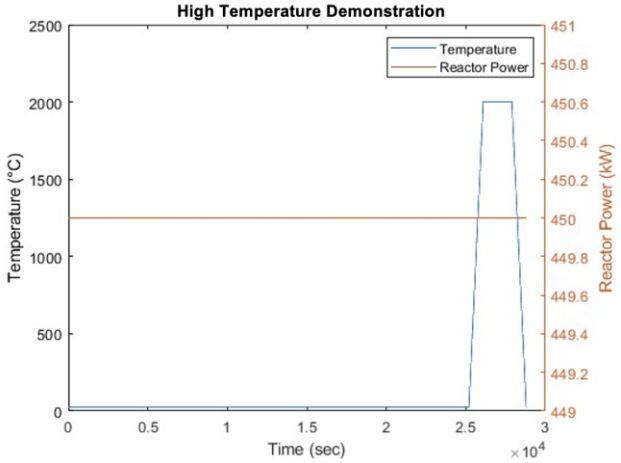

Fig. 6: Planned specimen region temperature variation in the last hour of irradiation.

This temperature will require around 600 W of delivered power to the heater. This experimental performance has been demonstrated during out-of-pile benchtop testing, but irradiation impacts on the heating capability of INSET have not yet been investigated. INSET is also being developed to accept flowing heated hydrogen gas for both in and out-of-pile tests. Currently, INSET can simulate the temperature and fluence seen in an NTP system, and it is being improved to simulate the hydrogen presence as well.

III.B Irradiation Test Plan

The second test implements the pressure transducers and platinum RTDs. The pressure transducers will be placed before the INSET heater to prevent measurement interferences that would come from increasing the temperature of the process fluid. Like the flow meter irradiation, the pressure within a flow path will be varied between a set maximum and minimum value. The temperature of the process fluid will be increased in steps and will not decrease over the irradiation period. This can

be seen in Figure 7 which is a visual representation of the described test plan.

The temperature level profile shown in Figure 7 will be achieved by electrically heating INSET using a maximum of 250W. The thermal energy will be carried away from the heater by radiation heat transfer followed by convection through flowing helium gas leading to the pressure sensor. Thermocouples located within the heater of INSET as well as along the helium flow path will be used to monitor the temperatures during the test.

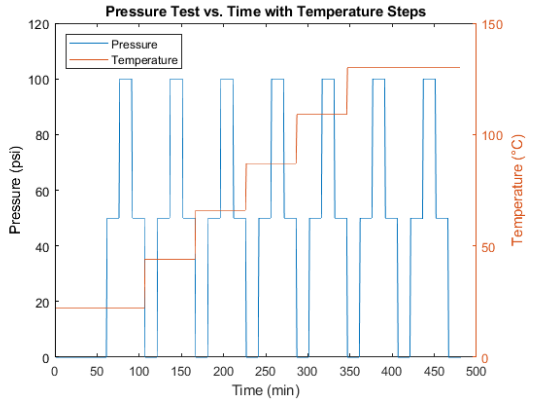

Fig. 7: Indication of pressure and temperature changes during the irradiation period.

IV. CONCLUSIONS

From the presented pre-irradiation characterization of a set of instruments and the irradiation test plan, important information can be determined regarding performance degradation due to radiation exposure. These effects are critical to ensuring the safe operation of nuclear rockets as they will have to perform for extended periods of time without maintenance. Further testing will require longer irradiation periods along with exposing instruments to higher temperatures. Initially these two components require separation to ensure that the cause of degradation can be determined. A combined test can then be completed to determine if there are additional degradation mechanisms that are due to simultaneous exposure to extreme temperatures and radiation. INSET will continue to serve as the steady state, high temperature, in-pile testbed to conduct these investigations.

REFERENCES

1. Gilles, W., *Instrumentation for Nuclear Rocket Engines.* IEEE Transactions on Nuclear Science, 1969. **16**(1): p. 266-270.
2. *Nuclear subsystem instrumentation*. 1971, ; Westinghouse Electric Corp., Pittsburgh, Pa. (USA). Astronuclear Lab. p. Medium: ED.
3. Steiner, T.R., E. Hutchins, and R.H. Howard, *Steady State In-Pile Nuclear Thermal Propulsion Experimental Testbed Initial Demonstration at the Ohio State University Research Reactor.* Nuclear Technology, 2021.

Nuclear and Emerging Technologies for Space
Sponsored by Oak Ridge National Laboratory, April 26th-30th, 2021.
Available online at https://nets2021.ornl.gov

A COOL MODEL TO ANALYZE HEAT DEPOSITION ON MTV PROPELLANT TANKS

Nicholas A. Morris[1], Dr. L. Dale Thomas, and Dr. Keith Hollingsworth

1301 Sparkman Dr., Huntsville, AL, 35899

Phone[1]: 256-824-5262 Email[1]: nam0021@uah.edu

Improved methods for storing liquid hydrogen in larger quantities and over longer periods of time in space are becoming progressively more critical as sights are once again set on Mars. Current storage methods involve the venting of vaporized hydrogen to space, with the consequence that significant amounts of hydrogen are wasted. Extra hydrogen must be stored to account for this loss resulting in unnecessary mass penalties. Eliminating this waste can reduce overall mission mass, extend mission range, and perhaps most importantly lower mission trip times and costs. This paper discusses the methods used to analyze the heat deposition on the Mars Transfer Vehicles' propellant tanks through its mission flight path and gives insight into how this analysis can be used in the selection of the appropriate thermal control methods given mission requirements.

I. Nuclear Thermal Propulsion

As mankind looks to Mars once again and considers the challenges of deep space exploration, it is evident that new propulsion technologies will be needed. Nuclear Thermal Propulsion (NTP) is an attractive 21st century option to propel human exploration missions to Mars and other deep space destinations[1] due to its favorable specific impulse which reduces overall trip times, total required mission mass, and costs. Reducing trip time is particularly important for human exploration missions because of harmful cosmic radiation. Although methods to shield against this radiation are being developed, simply spending less time exposed to the environment is readily achievable with propulsion systems such as NTP.

NASA's current design reference architecture[3] (DRA) considers the use of NTP as the main propulsion technology for both manned and unmanned Mars missions.

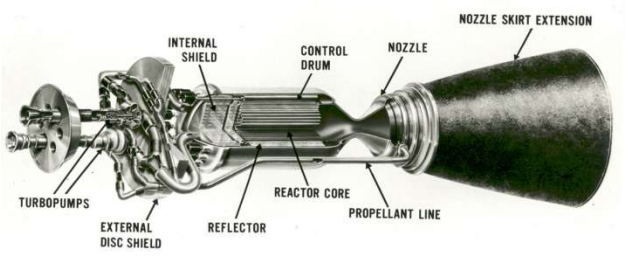

Fig. 1. An example of a nuclear thermal propulsion engine[1]

Common NTP engines (depicted in Fig. 1.) employ a nuclear reactor core to super heat pure hydrogen which is expanded through a rocket nozzle to obtain thrust. Liquid Hydrogen (LH_2) is the ideal propellant for NTP as it acts as both a coolant and a propellant. As a propellant, liquid hydrogen's low molecular weight yields a high specific impulse (I_{sp}) which exponentially reduces the overall propellant mass needed for the same ΔV mission requirement, shown by equation (1).

$$m_{propellant} = m_{inert}\left(e^{\frac{\Delta V}{Ispg_0}} - 1\right) \quad (1)$$

Alternatively, by maintaining the same amount of propellant mass, a higher I_{sp} results in an increased ΔV capability (see equation (2)). This, in turn, allows the selection of shorter transfer orbits or more simply put a decrease in overall trip time.

$$\Delta V = I_{sp} g_0 \ln\left(\frac{m_{propellant}}{m_{inert}} + 1\right) \quad (2)$$

Recent work[2] has shown that NTP ΔV capability can be increased even more by seeding hydrogen propellant with heavy noble gasses, such as Argon, further reducing overall trip times. The DRA, however, currently calls for the use of pure liquid hydrogen as the propellant for the NTP engine. *Due to the extremely low temperature hydrogen must be stored at, it makes an excellent standard in a model. The results of the thermal analysis of hydrogen will be applicable to nearly all space missions that use a cryogenic propellant in some capacity.*

II. Liquid Hydrogen

LH_2 is a cryogenic fluid and must be stored at low absolute temperatures, approximately 14-21 K (at two atmosphere), to prevent it from changing phase to a gas, an event here forth referred to as boil-off. Boil-off is problematic when storing LH_2 for two reasons. First, gaseous hydrogen is very difficult to pump. Second, when LH_2 changes to its gaseous form inside a pressure vessel, the pressure rises and can cause the vessel to exceed its limits and fail. To prevent this from occurring, the gaseous hydrogen must be vented to return the pressure of the vessel back to acceptable limits. As a result, the vented hydrogen is lost, and the overall effective employable amount of hydrogen propellant is decreased. To make up for this event (boil-off) more than the required amount of

hydrogen for an ideal zero-boil-off (ZBO) mission is needed.

This extra hydrogen is a major mass penalty. A 2011 study[4] (see Fig. 3.) shows that simply improving (reducing the amount of, not eliminating) boil-off is the single largest mass savings step in reaching the DRA's target mission mass. Completely eliminating boil-off would, of course, further increase mass savings.

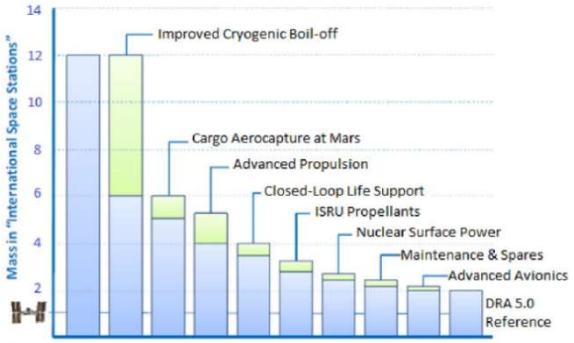

Fig. 3. Technology improvements needed to achieve DRA 5.0 reference total mission mass[4]. Improved Cryogenic Boil-off is shown as the largest step to achieve reference mass

Past works that analyze the thermal management of cryogenics in space have one key commonality, they all analyze relatively small volumes. Review of the relevant literature has been unable to identify a thorough analysis of a considerably large liquid hydrogen storage system in space, on "*the scale required for human planetary exploration,*" as JPL[11] describes it. Past research does not definitively conclude whether passive or active systems, as will be detailed in this paper, are more effective than the other. A thorough analysis of the MTV's propellant storage system through its proposed mission flight path will shed light on which of these systems are the most mass and energy-efficient and thereby the most cost effective. Results of this study will also be applicable to future deep space missions.

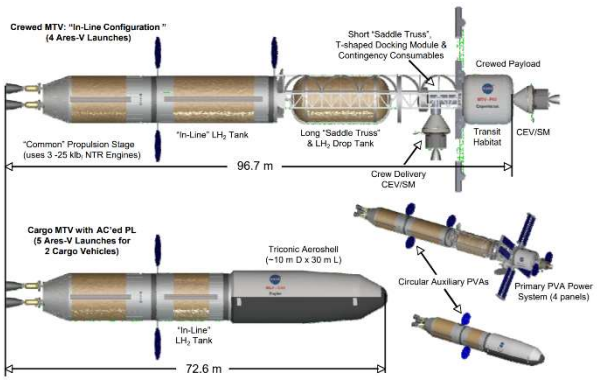

Fig. 2. The Mars Transfer Vehicle for crewed and cargo configurations as depicted in NASA's DRA 5.0

This paper provides a general analysis of a hydrogen propellant tank subjected to the environment of the Mars Transfer Vehicle (MTV), both natural and induced, in reference to the mission flight path laid out in the DRA. This paper also discusses methods to control the self-pressurization rate of the propellant tank to achieve zero-boil-off (ZBO). Non-ZBO methods and modifications to the MTV vehicle design and DRA flight path are reserved for future work. The Mars Transfer Vehicle is shown in Fig. 2. (ref. 3).

III. Thermal Analysis

A pressure control analysis using the first law of thermodynamics and the conservation of mass as done by Lin[6], et. al., shows that for a control volume that contains liquid-vapor contents, the homogenous self-pressurization (hsp) rate is,

$$\left(\frac{dP}{dt}\right)_{hsp} = \frac{\phi(Q_{net})}{V} \tag{3}$$

where ϕ is the internal energy derivative, and Q_{net} and V are the net heat into the system and the fixed cryogenic tank volume respectively. Furthermore, Lin points out that the pressure rise rate is governed by three key phenomena:

1. External heat leak
2. Fluid temperature stratification
3. Interfacial heat and mass transfer

External heat leak is evident in equation (3) (the variable Q_{net}) and will be the focus of the remainder of this paper. Both, fluid temperature stratification and interfacial heat and mass transfer have a lesser contribution and are thoroughly discussed in Lin's paper. Intermittent tank mixing is sufficient to make the effects of these two negligible.

For a constant density (thus a constant ϕ) and constant cryogenic tank volume, equation (3) suggests that tank pressure rises linearly with rising Q_{net}. In actuality, this is an exponential effect. As heat is added to the system and boil-off occurs, the overall propellant density decreases resulting in an exponential increase in ϕ and thus and exponential increase of dP/dt. However, for relatively slow pressure rates, ϕ can be taken as constant, and a linear model can be assumed.

A further analysis of Q_{net} depends entirely upon the environment in which the tank is located. For the MTV, the natural environment includes,

Q_{sol} solar radiation

Q_{alb} planetary albedo

Q_{IR} planetary infrared radiation

For an unprotected tank, the total heat load can be defined as the summation of these,

$$Q_{net} = Q_{sol} + Q_{alb} + Q_{IR} \quad (4)$$

To reduce the heat leak from the natural environment, the propellant tank is covered in low solar absorbance, high infrared emittance multi-layered insulation (MLI). MLI acts as a middleman between the natural environment and the propellant tank and the resulting reduced heat leak including the tank supports and subsystems can be expressed as,

$$Q_{net} = Q_{MLI} + Q_{struts} + Q_{piping} + Q_{mixer} - Q_{out} \quad (5)$$

where

Q_{struts} heat leak through supports

Q_{piping} heat leak through tank piping

Q_{mixer} heat add by tank mixer

Q_{out} heat radiated out or removed from the system

Another heat source to be considered, specifically for NTP, is the induced gamma ray and neutron emissions from the nuclear core. This has been modeled in prior work[5], and can be expressed as Q_{NTP} and added to (5),

$$Q_{net} = Q_{MLI} + Q_{struts} + Q_{piping} + Q_{mixer} + Q_{NTP} - Q_{out} \quad (6)$$

For Q_{net} to be zero, it can be seen that,

$$Q_{out} = Q_{MLI} + Q_{struts} + Q_{piping} + Q_{mixer} + Q_{NTP} \quad (7)$$

We can further express Q_{out} as its natural and induced components,

$$Q_{out_{nat}} + Q_{out_{ind}} = Q_{MLI} + Q_{struts} + Q_{piping} + Q_{mixer} + Q_{NTP} \quad (8)$$

Equation (8) implies two methods to achieve a Q_{net} equal to zero. The first, is to reduce the right side sufficiently to equal $Q_{out_{nat}}$. These are referred to as passive methods and require no induced heat removal (i.e. $Q_{out_{ind}} = 0$). Conversely, it is not always possible to sufficiently reduce the right side of equation (8) and $Q_{out_{ind}}$ must be greater than zero. When this occurs, Active methods of heat removal, such as cryocoolers, are necessary.

Finally, in some cases the $Q_{out_{nat}}$ can exceed the right side of equation (8) and heat would need to be added to the system. If Q_{mixer} is not sufficient, strip heaters (Q_{sh}) can be used. To account for this, equation (8) becomes,

$$Q_{out_{nat}} + Q_{out_{ind}} = Q_{MLI} + Q_{struts} + Q_{piping} + Q_{mixer} + Q_{NTP} + Q_{sh} \quad (9)$$

IV. Mars Transfer Vehicle

As the MTV moves through the phases of its mission, the heat loads detailed in equation (9) change significantly. To better analyze the problem and determine the optimum solution, it is important to define the MTV mission phases. The DRA proposed mission flight path is shown in figure four[3].

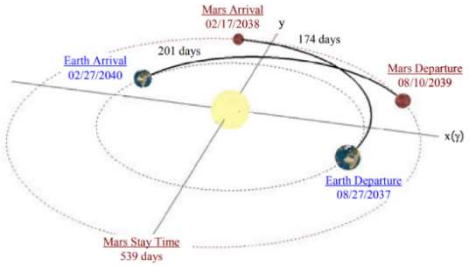

Fig. 4. Proposed flight path for 2037 crewed mission to Mars

The MTV is first scheduled to park in a cis-lunar orbit and await the crew. After some time, the MTV spends a lengthy period traveling through deep space on its way to Mars where it will park in Mars orbit and await its lengthy return trip back to Earth. These three phases are defined as:

Phase 1: Cislunar – pertaining to the Earth-Moon system, where the liquid hydrogen storage tanks spend a large fraction of the mission awaiting Phase 2 (journey to Mars). This phase is completed when the NTP engine completes its burn to enter Trans Mars.

Phase 2: Trans Mars/Earth – pertaining to the transition to Mars from Earth or vice versa, where the liquid hydrogen storage tanks coast through deep space.

Phase 3: Mars Orbit – pertaining to the orbit around Mars, where the liquid hydrogen storage tanks spend up to a year awaiting Phase 2 (return to Earth). This phase begins at the start of the second burn (to enter Mars orbit) and ends after the third burn (to enter Trans Earth).

In Phase 2, Q_{alb} and Q_{IR} are almost negligible and the right side of equation (8) can be reduced enough so that $Q_{out_{nat}}$ is greater and strip heaters will be needed. This has been shown in an analysis done by Plachta, et. al.[7] on the Titan Explorer mission. Plachta's work shows that by isolating the propellant tank's view to deep space, passive methods, such as sun shields, are enough to achieve ZBO for liquid hydrogen without the use of cryocoolers or other active heat removing systems.

As part of the same series of studies, Plachta reviews a Mars Sample Return Mission Concept[10] and concludes that due to the complications of shielding from both Q_{sol}

and Q_{alb} while in a planetary orbit, it may not be possible to reduce the right side of equation (8) sufficiently, thus the use of active heat removal systems such as cryocoolers would be required. The results of the studies are published in a report by JPL[11]. JPL adds in their conclusion that for *"very large systems of the scale required for human planetary exploration"* the results concluded by Lin above may not be applicable and implies that a further analysis would be needed.

For the model discussed in the next section, Aerojet Rocketdyne's MTV architecture will be used as a reference for the scale of the propellant tanks; 7 ft diameter by 11 ft in length. To simplify the thermal analysis, the tank will be modeled as a right cylinder with flat ends. However, future editions of the model will include the capability of selecting other geometries as well as importing .STL files for unique geometries.

Fig. 5. Tank geometry selection in the Thermal Analysis App

V. Thermal Analysis Model

Based off the author's previous work[12], A thermal analysis app to analyze heat deposition on the MTV's propellant tank was created using MATLAB and STK.

Fig. 6. Thermal Analysis App

The propellant tanks are discretized into isothermal nodes with area defined by user input. The top of Fig. 7 shows a loose mesh of the propellant tank to highlight the discretization method, whereas the bottom of Fig. 7 shows a more realistic mesh.

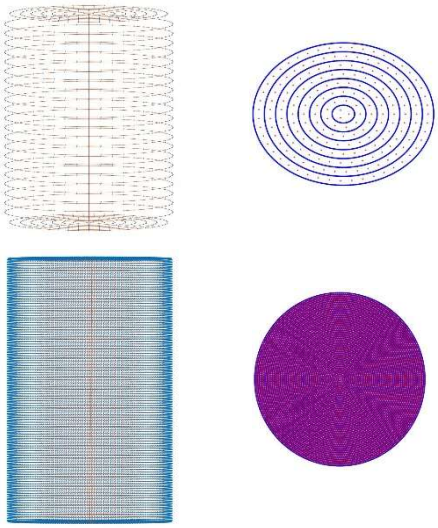

Fig. 7. (Top) Loose mesh on propellant tank. (Bottom) Realistic mesh.

Each isothermal node is modeled as a flat plate with a normal vector. AGI's STK is used in conjunction with MATLAB to determine the radiation view factors from a small flat plate to a spherical body[13], e.g. the Sun, Earth, and Mars. With these view factors, the nodes are subjected to a back-loss model that computes their steady-state temperature considering a hemispherical enclosure of N black bodies + 1 gray body (the flat plate) and the heat transfer between a user defined number of gray shields and the constant steady-state temperature of the liquid hydrogen. Future revisions will include lateral heat transfer between nodes.

This method provides the temperature profile of the tank and the nodal heat flux. To determine the effects on the tank, the user can define a number of "slices" to break the tank up into. The average temperature and total power for each these slices are then determined and graphed for diagnostic purposes. Figures 8 through 10 show an example of these plots.

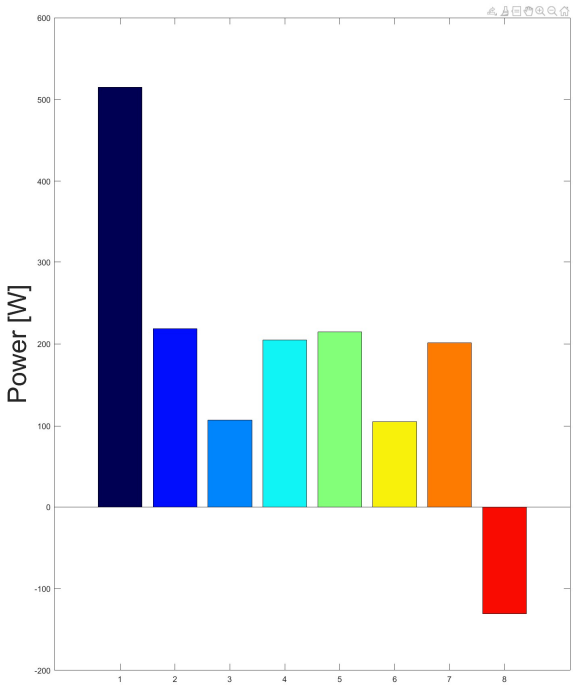

Fig. 8. Power versus Slice

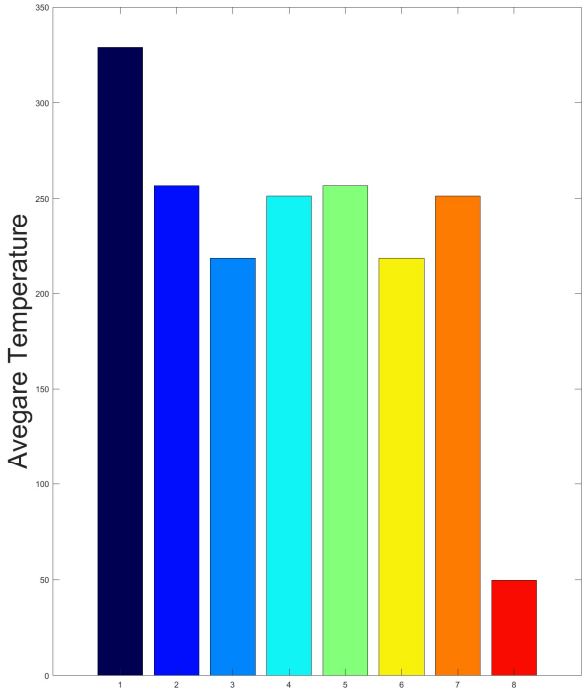

Fig. 9. Average Temperature versus Slice

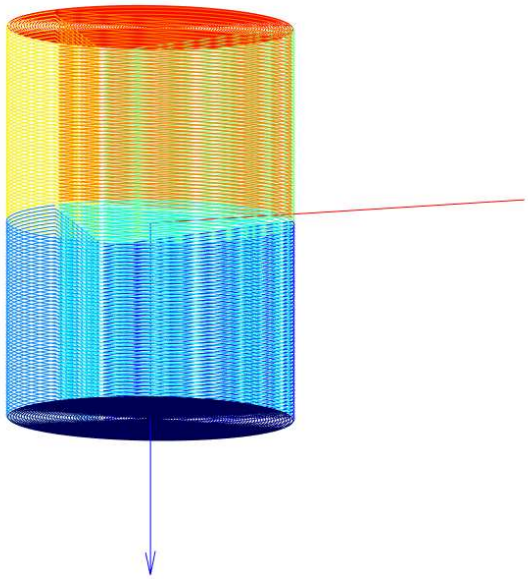

Fig. 10. Color map of tank with radiation source vectors

The left side shows the power through each slice and the sum of these slices is the total power for the tank. The right side shows the average temperature of each slice. The slices are numbered and color coated to map each slice to a reference image at the top if the plot which also shows the vectors to the applicable radiation sources, in this example case, the Sun and the Earth. These diagnostic plots allow the user to see, in this example, that slice 1, the slice facing the Earth, has the highest temperature and allows most into the tank. Thus, the user should take precautions to mitigate the heat transfer on this slice.

Furthermore, this method allows the user to either input an R-value and have the system's overall heat flux calculated, or model the system as a black box thermal protection system to determine the required R-value to achieve zero boil-off. These R-values can also be compared to the R-values of various thermal control systems to find a suitable system. Trade studies will be performed based on mass, power consumption, complexity, and overall mission costs to determine the best system for the MTV during each phase and for the entirety of the mission.

Presently, this model is being validated by professional review and a comparison of simple scenarios modeled in Thermal Desktop.

VI. Conclusions

The largest mass saving step in the design of the Mars Transfer Vehicle is the elimination of the vented hydrogen, boil-off, by achieving steady-state conditions. It is thus the purpose of this study to determine if the hydrogen aboard the MTV can be maintained at a steady state for the duration of the MTV's mission and to gain insight on thermal protection system required to do so. If this can be achieved, mission costs, design complexity, and, perhaps most importantly, trip times to Mars would be greatly reduced. The impact of this research is not limited to the MTV or to hydrogen. Virtually all in-space propulsion systems rely on some sort of liquid to operate. Because hydrogen is one of the coldest liquids used, the results if this study will be applicable to any cryogenic liquid that is stored at a higher temperature. This is especially useful for chemical rocket engines which commonly use liquid oxygen or liquid methane. The methods developed here will be applicable to all such cases.

VII. Future Work

Future work includes determining if the hydrogen can be kept at a steady state using passive systems only and what the tradeoffs will be versus using active thermal control methods or combinations of active and passive thermal control methods. Additionally, the model will be expanded to include transient analysis. The model will also be integrated with a system model of the Mar Transfer Vehicle[14] to provide information on the status of the propellant tanks.

ACKNOWLEDGMENTS

This work was supported by the National Aeronautics and Space Administration.

REFERENCES

1. Hall, L. Nuclear Thermal Propulsion: Game Changing Technology. NASA. http://www.nasa.gov/directorates/spacetech/game_changing_development/Nuclear_Thermal_Propulsion_Deep_Space_Exploration. Accessed Dec. 4, 2019.
2. D. Nikitaev & D. Thomas, "Seeded Hydrogen in Nuclear Thermal Propulsion Engines," AIAA Journal of Spacecraft and Rockets. (submitted)
3. Humans Exploration of Mars Design Reference Architecture 5.0. https://www.nasa.gov/pdf/373665main_NASA-SP-2009-566.pdf.
4. Braun, D. B. "Investments in Our Future: Exploring Space Through Innovation and Technology." slide 9.
5. A. Aueron, D. Thomas, & J. Cassibry, "Analytical Modeling of Radiation Attenuation and Heat Deposition in Propellant for Nuclear Thermal Rockets," AIAA Journal of Spacecraft and Rockets, March 2019.
6. Lin, C.-S., Van Desar, N. T., and Hasan, M. M. "A Pressure Control Analysis of Cryogenic Storage Systems." p. 12.
7. Plachta, D. W., Christie, R. J., Jurns, J. M., and Kittel, P. "Passive ZBO Storage of Liquid Hydrogen and Liquid Oxygen Applied to Space Science Mission Concepts." Cryogenics, Vol. 46, No. 2–3, 2006, pp. 89–97. doi:10.1016/j.cryogenics.2005.11.012.
8. Plachta, D. W., Christie, R. J., Feller, J. R., and Johnson, W. L. Cryogenic Boil-Off Reduction System Testing. Presented at the 50th AIAA/ASME/SAE/ASEE Joint Propulsion Conference, Cleveland, OH, 2014.
9. Guzik, M. C., and Tomsik, T. M. "An Active Broad Area Cooling Model of a Cryogenic Propellant Tank with a Single Stage Reverse Turbo Brayton Cycle Cryocooler." TFAWS 2011, 2011.
10. Plachta, D. W., Christie, R. J., Jurns, J. M., and Kittel, P. "ZBO Cryogenic Propellant Storage Applied to a Mars Sample Return Mission Concept." AIP Conference Proceedings, Vol. 823, No. 1, 2006, pp. 205–212. doi:10.1063/1.2202418.
11. Guernsey, C., Baker, R., Plachta, D., and Kittel, P. Cryogenic Propulsion with Zero Boil-Off Storage Applied to Outer Planetary Exploration. Presented at the 41st AIAA/ASME/SAE/ASEE Joint Propulsion Conference & Exhibit, Tucson, Arizona, 20
12. Morris, N. A., Thomas, L. D., and Hollingsworth, D. K. "Stay Cool—Alternatives for Long-Term Storage of Large Quantities of Liquid Hydrogen on a Mars Transfer Vehicle." *Nuclear Technology*. https://doi.org/10.1080/00295450.2020.1819157.
13. Ballinger, J. C., Elizalde, J. C., and Christensen, E. H. "Thermal Environment of Interplanetary Space." SAE Transactions, Vol. 70, 1962, pp. 512–525.
14. Nikitaeva, D., Thomas, L. D., Aueron, A. L., Kumar, S., and Nikitaev, D. Nuclear Thermal Propulsion Spacecraft Integrated System Model. In AIAA Scitech 2021 Forum.

Nuclear and Emerging Technologies for Space
Sponsored by Oak Ridge National Laboratory, April 26th-30th, 2021.
Available online at https://nets2021.ornl.gov

HELICON INJECTED INERTIAL PLASMA ELECTROSTATIC ROCKET

Rohan Puri[1], George H. Miley[1], Raul Patino[1], Raad Najam[1], and Erik Ziehm[1]

[1]*Fusion Studies Lab, University of Illinois at Urbana-Champaign, Urbana, IL, 61801*

Primary Author Contact Information: 217-650-9738 & rohanp5@illinois.edu

Helicon Injected Inertial Plasma Electrostatic Rocket (HIIPER) is an electric propulsion system being developed at the University of Illinois Urbana-Champaign. It is considered as a steppingstone towards a nuclear fusion propulsion system. This study summarizes the various performance parameters of the device along with ongoing research and future scope of work. Preliminary computational results on plasma dependence on helicon tube dimensions are also presented and discussed. The paper lays the groundwork for possible future upgrades of the experimental setup.

I. INTRODUCTION

HIIPER started as a prototype deep space electric propulsion system. Its conceptual design involves two main stages – plasma generation using Helicon waves and its (plasma) extraction into an inertial electrostatic confinement (IEC) fusion chamber. The latter is accomplished with the help of electrostatic grids.

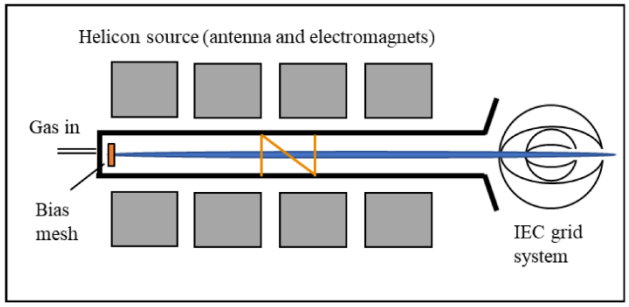

Fig. 1. HIIPER Schematic

I.A. Helicon Theory

A helicon wave is a circularly polarized, right-handed electromagnetic wave, that is a type of whistler wave [1]. It differs from a whistler wave in a way that it has a lower frequency and is formed inside an antenna wrapped cylindrical tube [2]. A magnetic setup is used to generate an axial field which completes the plasma generating setup of the helicon tube.

Parameters affecting the plasma density of the helicon setup are – applied radio frequency (rf) power, axial magnetic field (mf), helicon tube radius, tube shape and the internal pressure due to neutral gas. For a given mf, a minimum rf power is required to excite the helicon waves and generate plasma [3]. Rf frequency, which alters the ionization of the gas, is generally kept constant at 13.6 MHz [4]. Out of the three modes of plasma, i.e. inductively coupled mode, capacitively coupled mode and helicon wave mode, highest ionization occurs in the helicon mode.

I.B. IEC Fusion Theory [5]

An IEC fusion chamber consists of, essentially, a metal grid positioned inside a grounded vacuum chamber. The grids are applied with negative potential in the kilovolts range which ionizes the gas injected inside the chamber from Paschen breakdown. Mainly two types of grids have been studied – spherical and cylindrical.

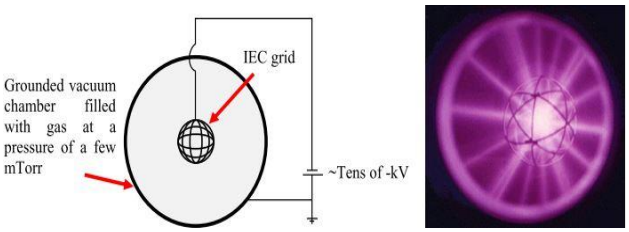

Fig. 2. Left: IEC fusion schematic. Right: IEC star mode.

Prior IEC fusion studies concluded with three types of discharge modes being observed. The "star" mode consisting of microchannels of ion dominated beams oscillating throughout the chamber. The "central spot" mode where the ions are confined in the center of the cathode. Finally, the "halo/jet" mode consisting of a non-neutral electron dominated plasma. Initial studies done at the University of Illinois involved investigating the "halo" mode at low pressure [6,7]. Further studies added an extractor grid at the end of the IEC cathode grid [8]. The ion current was being affected by the gas pressure inside the IEC fusion chamber. This pressure dependence was eliminated by adding a helicon injection source to the IEC fusion setup.

I.C. Salient Features of HIIPER

IEC chamber provides a confinement mechanism for fusion space propulsion research. The cathode grids also generate a stream of high energy electron which partially neutralizes the exhaust plume [9]; thus preventing charge development on the external surfaces of the spacecraft. Also, a meshed electrostatic grid (bias grid) is placed at the upstream end of the helicon tube which applies a positive

voltage to the plasma. This has shown a twofold effect – higher ion flow rate through the tube and increased helicon-IEC coupling efficiency [10]. The exact relation between bias grid potential and plasma quality is currently being studied, and the mechanism along with the results will be explained in future publications.

II. COMPUTATIONAL STUDIES

HIIPER models have been designed and simulated using commercial Multiphysics software COMSOL [11]. Primary studies involved model development and validation using experimental data. Now the model is being used to optimize the system and test possible upgrades for HIIPER. Adding a magnetic nozzle (MN) at the final stage of HIIPER is being investigated. Charged particle tracing is being used to understand particle trajectories and various particle collisions inside HIIPER.

II.A. Helicon Model

Magnetic field (mf) and plasma electromagnetic waves are used to replicate the helicon-IEC setup of HIIPER. Charged particle tracing was used to understand ion trajectories inside HIIPER and find the position of ion loss. The model is divided into three parts as shown in the following figure.

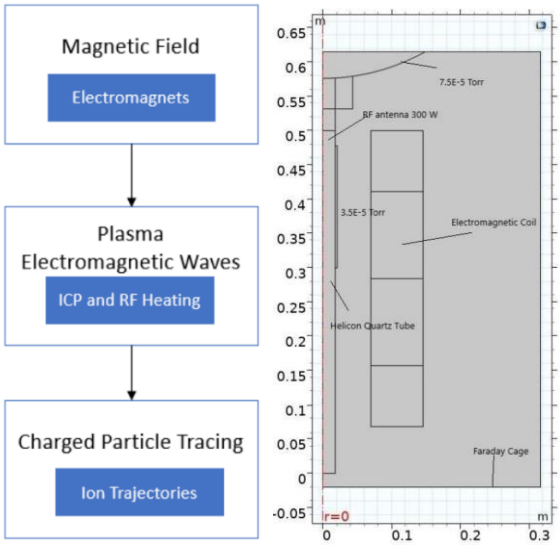

Fig. 3. Computational flowchart and model [12].

II.B. HIIPER-MN Integrated Model

These simulations were carried out, as a preliminary proof of concept, to observe changes in the exhaust ion velocities and kinetic energy after passing through a magnetic nozzle. A general trend was established between the axial magnetic field and ion velocities.

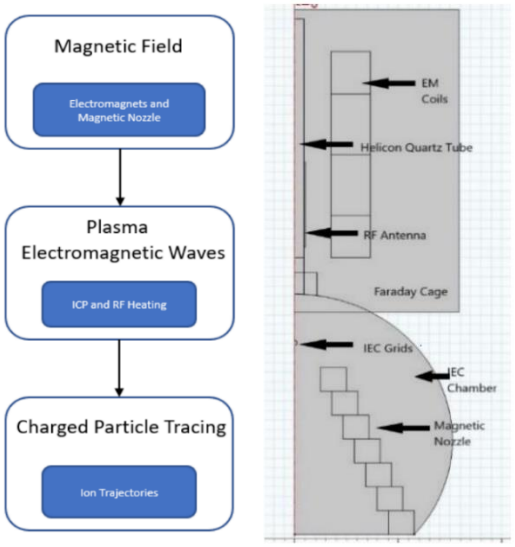

Fig. 4. Computational flowchart and model [13].

II.C. Results

II.C.1. Electron Motion inside IEC Chamber

This was a qualitative study done to observe the electron motion for "star" and "jet/halo" mode of operation and inspect different designs to influence the electron motion to our benefit. It is observed inside the blue circle in Fig. 5 that electron density is higher towards the asymmetric exhaust. Electrons generated in these discharges neutralize the exhaust plume, an intrinsic advantage of HIIPER, to avoid charging up the outer walls of the system.

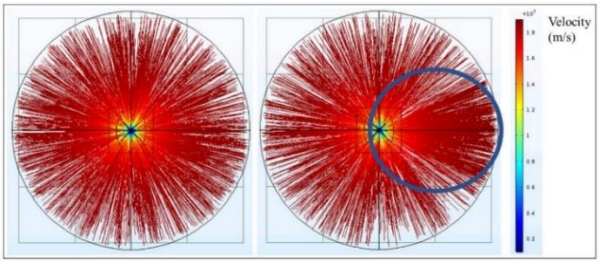

Fig. 5. Electron trajectories for left: "star" mode and right: "halo" mode [14].

II.C.2. Ion Motion inside IEC Chamber

This was also a qualitative study to see ion trajectories during the "jet/halo" mode of operation. The number of ions hitting the grid wire, which depended on the applied IEC voltage, were directly proportional to the number of secondary electrons being generated. This indicated that electrons were primarily being generated due to ion grid collision and future studies should include grid erosion in the model. Secondly, it is also noticed that ions lose velocity while leaving the IEC grid setup. MN study, described in this paper, overcomes the abovementioned shortcoming.

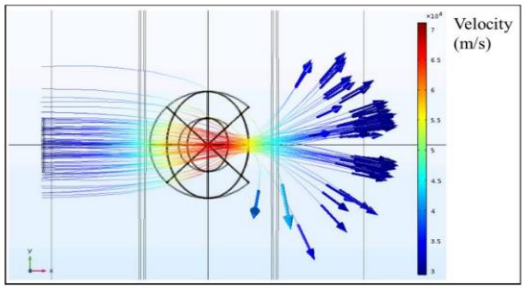

Fig. 6. Ion trajectories for "halo" mode [14].

II.C.3. Addition of Magnetic Nozzle to HIIPER

This study involved testing out an electromagnetic setup right after the IEC grid to check if ion kinetic energy (or velocity) is conserved, if not increased. The simulations were carried out at different axial magnetic field values. It was observed that ion velocities increased roughly by 27 % when the magnetic field was 1.4 T. It was also seen that the percentage of increase had a direct relation with initial ion velocities and applied magnetic field.

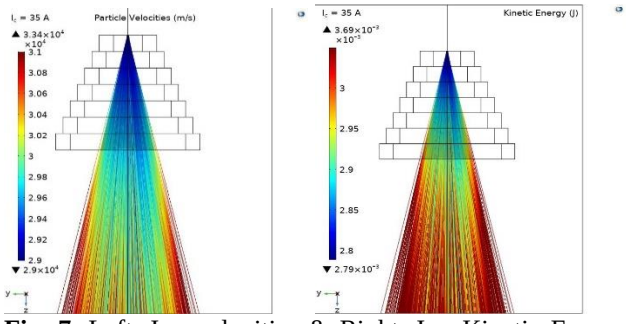

Fig. 7. Left: Ion velocities & Right: Ion Kinetic Energy after passing through a MN [10,13].

II.C.4. Ion Loss due to Collision with Walls in Helicon

Charge particle tracing results revealed that most of the ions generated inside the helicon are lost to the walls of helicon-IEC chamber coupling. It can also be observed by noticing the loss of ion density downstream end of the helicon tube. This has proven to be the main cause of low thrust values of HIIPER.

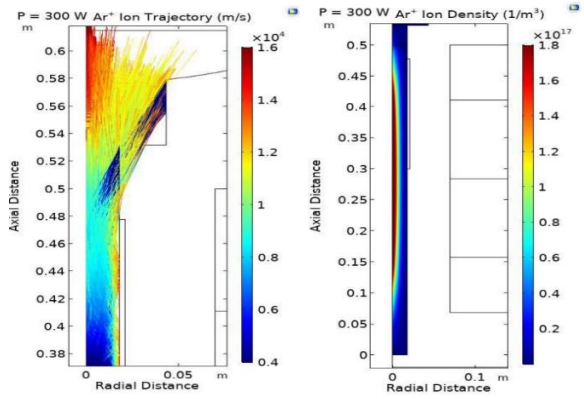

Fig. 8. Left: Ion Trajectory & Right: Ion Density [10,12].

III. EXPERIMENTAL INVESTIGATIONS

HIIPER experimental facility consists of an m = +1 configuration, 3.81 cm outer diameter helicon quartz tube; surrounded by an electromagnet setup capable of generating an axial magnetic field of up to 1.2 T. The quartz tube is connected to a 61 cm inner diameter stainless steel vacuum chamber, that also acts as the anode for the IEC fusion chamber. With argon as the propellant and plasma being generated using 300 W rf power supplied to the helicon, the system pressure remained at 6 mTorr. IEC cathode grids, made of nickel wire of 0.8 mm diameter, were used to extract the plasma from the helicon tube.

Langmuir probe diagnosis is used to measure ion density, based on quasi neutrality condition, and estimate electron temperature and thermal velocity of the ions. Retarding potential analyzer (RPA) is used to measure most probable ion energy and approximate the electron energy distribution of HIIPER. A torsional pendulum thrust balance has been used for prior force measurements [14], but new methods are being investigated for more accurate diagnosis of the thrust.

Performance aspects of HIIPER have been published in Ref. [10, 14] and it has been observed that the highest value of ion densities is achieved with helicon axial magnetic field set to 90 Gauss. The ion densities are also directly proportional to the applied RF power and IEC grid voltage.

III.A. Relation Between Ion Density and RF Power

Ion densities were measured at two locations to confirm the charged particle tracing results – inside helicon and after the helicon-IEC coupling. The IEC grid voltage was set to negative 3 kV and bias grid was left floating with 90 Gauss external magnetic field. The figure below depicts, inside helicon, the ion densities are well above 10^{17} m^{-3}. Comparing it to the ion densities measured after the coupling, the values were at least an order of magnitude higher inside the helicon. This confirmed that ions were being lost to the walls of the coupling.

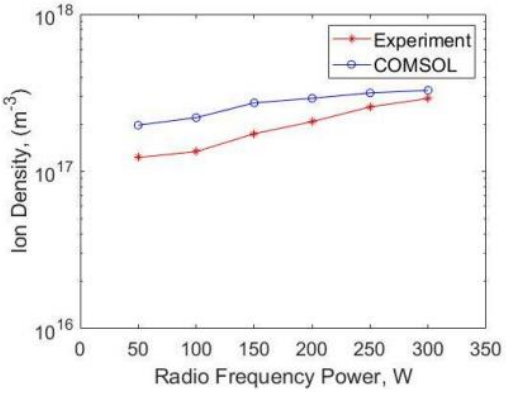

Fig. 9. Ion density vs RF power inside helicon [10].

III.B. Relation Between Thrust and RF Power

With maximum ions being lost to the coupling walls, the thrust generated was only in micronewton range. The figure below shows these values for 2 different IEC grid voltages. These measurements will be updated in the future after solving the ion wall losses to the coupling.

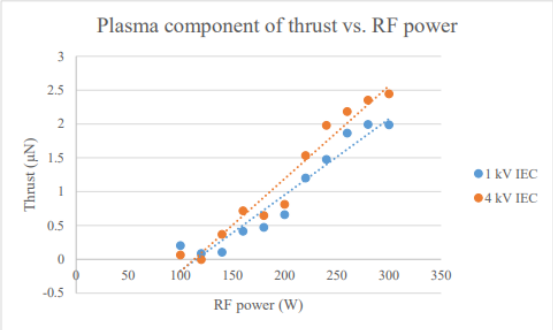

Fig. 10. Thrust vs RF power [14].

IV. CONCLUSIONS AND FUTURE WORK

This paper summarizes the results achieved in previous HIIPER research. Plasma of ion densities between 10^{17} m^{-3} to 10^{18} m^{-3} are easily generated with rf power anywhere above 200 W. Beam of high energy electrons is pushed out of the system, partially neutralizing the ions, due to internal electrostatic field of the IEC grids. Electron energies were observed to depend on IEC cathode grid voltage whereas Ion energies depended on helicon rf power and bias grid voltage. These experiments [7-11] have established the fact that increasing rf power or negative IEC grid voltage also increases the ion density of the generated plasma. A convergence between computational results and experimental results is seen with more sophisticated diagnosis method and equipment. Numerical estimates suggest that HIIPER can generate thrust in the order of milli Newtons once the ion wall losses are eliminated [10].

Ongoing computational studies focus on establishing a relation between helicon tubes L/D ratio and generated plasma density for a given rf power. Current experimental research involves two main points of interest – Using a helicon bias plate to collimate the plasma [15] and, potentially, prevent ion wall losses and carrying out thrust measurements with a standalone model of HIIPER.

REFERENCES

1. F. Chen, "Plasma ionization by helicon waves, "*Plasma Physics and Controlled Fusion*, vol. 33, no. 4, pp. 339-364, 1991.
2. F. Chen, "Experiments on helicon plasma sources," *Journal of Vacuum Science & Technology A*, vol. 10, no. 4, pp. 1389-1401, 1992.
3. J.-H. Kim and H.-Y. Chang, "A study on ion energy distribution functions and plasma potentials in helicon wave plasmas," *Phys. Plasmas*, vol. 3, no. 4, pp. 1462-1469, 1996
4. R. M. Magee, M. E. Galante, N. Gulbrandsen, D. W. McCarren and E. E. Scime, "Direct measurements of the ionization profile in krypton helicon plasmas," *Phys. Plasmas*, vol. 19, p. 123506, 2012.
5. G. H. Miley and S. K. Murali, *Inertial Electrostatic Confinement (IEC) Fusion Fundamentals and Applications*, New York: Springer, 2014.
6. B. A. Ulmen, "Formation and Extraction of a Dense Plasma Jet from a Helicon-Plasma Injected Inertial Electrostatic Confinement Device", *Ph.D. Dissertation*, NPRE Dept., University of Illinois at Urbana-Champaign, Champaign, IL, 2013.
7. D. Ahern, B. Bercovici, G. H. Miley, G. Chen, B. Ulmen and P. Keutelian, "Advances on the Helicon Injected Inertial Plasma Electrostatic Rocket," *AIAA SPACE 2014 Conference and Exposition*, San Diego, CA, AIAA 2014-4172, 2014.
8. D. Ahern, J. Bowman and G. H. Miley, "Current Status of the Helicon Injected Inertial Plasma Electrostatic Rocket," *62nd AIAA/SAE/ASEE Joint Propulsion Conference*, Salt Lake City, UT, AIAA 2016-4734, 2016.
9. D. Ahern, G. H. Miley, "Experimental Analysis of the Helicon Injected Inertial Plasma Electrostatic Rocket (HIIPER)," *54th AIAA/SAE/ASEE Joint Propulsion Conference*, Cincinnati, OH, 2018.
10. R. Puri, G.H. Miley, Study of the Helicon Injected Inertial Plasma Electrostatic Rocket (HIIPER) Integrated with a Magnetic Nozzle, *ASCEND 2020*, November 16-18, 2020, Virtual Event.
11. COMSOL Multiphysics® v. 5.4. www.comsol.com. COMSOL AB, Stockholm, Sweden.
12. R. Puri, G.H. Miley, "Helicon Optimization Within the HIIPER Space Engine Through the Charged Particle Tracing Module", *COMSOL Conference*, 2020.
13. R. Puri, G.H. Miley, "Computational Study of Adding Magnetic Nozzle in HIIPER Using Multiphysics Module", *COMSOL Conference*, 2020.
14. D. Ahern, "Investigation of a Space Propulsion Concept using Inertial Electrostatic Confinement," *Ph.D. Dissertation*, NPRE Dept., University of Illinois at Urbana-Champaign, Champaign, IL, 2018.
15. R. M. Winglee and et. al, "Advances in High Power Beamed Plasma Propulsion," *38th AIAA Plasmadynamics and Lasers Conference*, Miami, FL, 2007.